

COMPARATIVE ASSESSMENT OF NON-CONSERVATIVE AND CONSERVATIVE RANS FORMULATIONS FOR COASTAL APPLICATIONS INVOLVING BREAKING WAVES

Shaswat Saincher¹ and V. Sriram¹

Two-phase Reynolds Averaged Navier-Stokes (RANS) simulations of breaking waves are susceptible to an unphysical thickening of the plunging crest. This is often times incorrectly attributed to deficiencies in the interface capturing scheme although, in reality, the issue stems from the nature of density treatment in momentum advection. If the density is considered face-centered in the advection term, the resulting formulation is conservative whilst if the density is modeled as a cell-centered quantity, the resulting formulation is non-conservative. Despite both approaches having been extensively applied to wave-breaking simulations in the literature, there is no study comparing both formulations for the same breaking scenario. In the present paper, we extensively compare both formulations for several depth- and steepness-induced breaking problems simulated using our in-house solver: IITM-RANS3D. Through these simulations, our work successfully addresses the following research questions: (a) how and why density treatment affects the physics of overturning and subsequently the plunging jet's topology and (b) what are the implications of choosing a particular formulation for simulating a violent wave-structure interaction scenario?

Keywords: two-phase, wave-breaking, density treatment, wave-structure-interaction, IITM-RANS3D.

MOTIVATION

The accuracy and fidelity of two-phase Reynolds Averaged Navier-Stokes (RANS) simulations of coastal engineering problems involving breaking waves is critically dependent on the nature of density treatment at the air-water interface. If the density is considered as a cell-centered quantity in the momentum advection term, the resulting formulation is termed as non-conservative whilst considering the density as a face-centered quantity results in a conservative formulation.

The non-conservative formulation is considered advantageous from the standpoint of numerical stability and is thus preferred for two-phase RANS simulations. The numerical stability primarily stems from the smearing of the density jump (which is 1:800 for air-water two-phase flow) across the interface. However, when applied to breaking waves, the non-conservative formulation leads to an unphysical thickening of the plunging jet. This is substantiated by a brief literature review of Navier-Stokes-based simulations of breaking waves reported in Table 1. It is seen that, for two-phase RANS, there is a strong correlation between the formulation of momentum advection and the resulting topology of the plunging jet. It is also worth noting that this issue doesn't manifest if a single-phase or mesh-free method is used to solve the Navier-Stokes equations (Sriram et al., 2014).

Authors	Momentum advection	No. of phases	Type of wave	Thickening of the plunging jet observed?
Sriram et al. (2014)	Lagrangian	1	Solitary ($H/d = 0.45$)	No
Xie (2015)	Conservative	2	Solitary ($H/d = 0.45$)	No
Chella et al. (2017)	Non-conservative	2	Solitary ($H/d = 0.33$)	Yes
Saincher and Banerjee (2018)	Non-conservative	2	Regular (Stokes V)	Yes
Aggarwal et al. (2019)	Non-conservative	2	Irregular (Bretschneider)	Yes
Chella et al. (2019)	Non-conservative	2	Regular (Stokes V)	Yes
Aggarwal et al. (2020)	Non-conservative	2	Irregular (JONSWAP)	Yes
Xie and Stoesser (2020)	Conservative	2	Solitary ($H/d = 0.5$)	No
Desmons and Coquerelle (2021)	Conservative	2	Regular (Airy)	No
Xie and Lin (2022)	Conservative	2	Solitary ($H/d = 0.45$)	No

Replicating the physics of shallow-water breaking becomes especially challenging in this regard since the overturning of the crest occurs over a large distance. This issue, oftentimes incorrectly attributed to the interface tracking scheme, is exclusive to two-phase RANS solvers and can only be rectified using a conservative formulation. As evidenced from Table 1, both non-conservative as well as conservative RANS simulations of breaking waves have been extensively documented in the literature. However, to the best of the authors' knowledge, there is no paper comparing both formulations for the same breaking scenario. In the present work, we propose to fill this research gap by addressing two pertinent questions: (a) how and why does the physics of breaking change with density treatment? and (b) what are the implications of density treatment on simulations involving breaking waves impacting a coastal structure?

¹ Department of Ocean Engineering, IIT Madras, Chennai, Tamil Nadu, 600 036, India.

APPROACH OF INVESTIGATION

We implement the two approaches of advection treatment to our in-house CFD solver IITM-RANS3D (Saincher and Sriram, 2022a; 2022b). Both formulations are then applied to simulate: (1) solitary wave breaking over a plane-sloping beach, (2) solitary wave breaking over complex bathymetry, (3) steepness-induced breaking of a focusing wave and (4) regular waves shoaling and impacting a recurved seawall at prototype scale (1:1).

For the aforementioned test cases, the breaking wave topology as well as the velocity field induced in both air and water phases are compared across the non-conservative and conservative formulations. In addition, for problems (1) through (3), the change in fluid mass within a cell estimated by the interface tracking scheme is compared against that estimated during momentum advection. This change is found to be inconsistent for non-conservative RANS which causes air to induce an unrealistically large deceleration on water in turn leading to unphysical thickening of the plunging jet. For conservative RANS, the fluid mass change between interface tracking and momentum advection is more consistent thus precluding said unphysical deceleration of the plunging jet.

The implications of these findings are further investigated through problem (4) in context to breaking waves interacting with a coastal structure. Although the hydrodynamic pressure variation obtained from both formulations is comparable, conservative RANS was found to be numerically more stable as multiple violent breaker-structure-interaction cycles could be simulated.

NUMERICAL MODEL

The CFD solver IITM-RANS3D has been recently developed in-house at the Department of Ocean Engineering, IIT Madras to simulate complex interactions between waves and fixed/moving/floating structures. Wave-structure interaction (WSI) is modeled as a multiphase flow within the finite-volume framework using the single-fluid formulation. The RANS equations governing the evolution of the mean velocity field \vec{V} are written in integral form as:

$$\int_S \vec{V} \cdot d\vec{S} = 0 \quad (1)$$

$$\int_V \frac{\partial(\rho^*\vec{V})}{\partial t} dV + \int_S (\rho^*\vec{V}\vec{V}) \cdot d\vec{S} = - \int_V \vec{\nabla} p dV + \int_S (\mu^*\vec{\nabla}\vec{V}) \cdot d\vec{S} + \int_V \rho^* \vec{g} dV \quad (2)$$

where, p is the pressure, ρ^* and μ^* are the mixture density and viscosity respectively and \vec{g} is the gravitational acceleration vector. The solid is modeled as a highly viscous ‘‘third’’ phase alongside air and water using the Fast-Fictitious Domain (FFD) method. In FFD, the high viscosity attributed to the solid phase enables implicit imposition of the no-slip condition over the solid boundary (Mirzaii and Passandideh-Fard, 2012). The mixture properties are obtained from the liquid and solid volume fractions (f_ℓ and f_s) invoking a single-fluid formulation:

$$\begin{aligned} \rho^* &= f_\ell \rho_\ell + f_s \rho_s + (1 - f_\ell - f_s) \rho_g \\ \mu^* &= f_\ell \mu_\ell + f_s \mu_s + (1 - f_\ell - f_s) \mu_g \end{aligned} \quad (3)$$

where the subscripts ℓ , s and g denote the liquid (water), solid (structure) and gas (air) phases respectively. Volume-fraction (f) evolution is governed by the hyperbolic transport equation:

$$\int_V \frac{\partial f}{\partial t} dV + \int_S (\vec{V} f) \cdot d\vec{S} = \int_V f(\vec{\nabla} \cdot \vec{V}) dV \quad (4)$$

Equation (4) is solved using the operator-split CICSAM (OS-CICSAM) scheme where the interface advection has been made direction-split to increase the computational efficiency of the algebraic VOF computations (Saincher and Sriram, 2022a). In order to maintain strong pressure-velocity coupling, the U, V, W -momentum cells are back-staggered by half a cell-dimension from the p, f -cells. IITM-RANS3D is one-way coupled with another in-house developed Fully Nonlinear Potential Theory (FNPT) code: IITM-FNPT2D (Sriram et al., 2006) thus facilitating energy-preserving simulation of wave-hydrodynamics in large domains over long time (Saincher and Sriram, 2022b).

IMPLEMENTATION OF CONSERVATIVE AND NON-CONSERVATIVE ADVECTION IN RANS

The main focus of the present work is how the advection term $\int_S (\rho^*\vec{V}\vec{V}) \cdot d\vec{S}$ is handled in the momentum equation and how it affects breaking wave simulations. Two different approaches of treating momentum advection are illustrated in Figure 1 by means of a 1-D example. Consider a U -momentum cell ‘‘P’’ (cell-center indicated with yellow in Figure 1) for which the momentum advection term is to be written in discrete form.

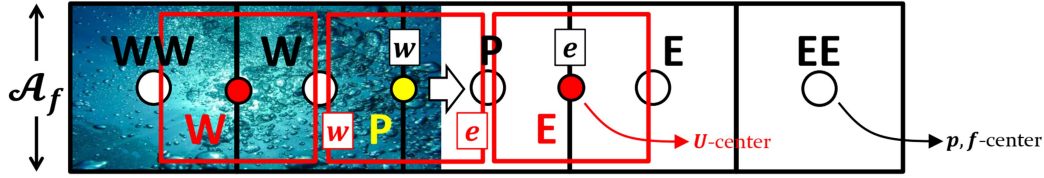


Figure 1. One dimensional advection scenario where the water-phase moves west to east over a staggered Navier-Stokes mesh. The p, f -cells are shown in black and the U -momentum cells in red. Uppercase and lowercase letters denote cell-centers and face-centers respectively.

If ρ^* is interpreted as a cell-centered quantity, it leads to the non-conservative form of momentum transport (Xie, 2011):

$$\rho^* \int_S (U\vec{V}) \cdot \overline{d\vec{S}} = \rho_p^* (U_e^a U_e - U_w^a U_w) \mathcal{A}_f \quad (5)$$

where the “advected” quantity is denoted by superscript “a” and \mathcal{A}_f is the face area. On the other hand, if ρ^* is interpreted as a face-centered quantity, it leads to the conservative form of momentum transport (Xie, 2011):

$$\int_S (\rho^* U\vec{V}) \cdot \overline{d\vec{S}} = (U_e^a m_e - U_w^a m_w) \mathcal{A}_f \quad (6)$$

where m_e is the mass-flux through the east face of the U -momentum cell which is evaluated as the mean of the mass-fluxes through the adjacent “E” and “P” cell-centers over the U -grid (highlighted in red in Figure 1). Thus:

$$m_e = 0.5((\rho^* U)_E + (\rho^* U)_P) \quad (7)$$

The critical aspect in evaluating $(\rho^* U)_E$ and $(\rho^* U)_P$ in equation (7) is that neither the density nor velocity should be interpolated at any stage (Xie, 2011). Upon comparing the discrete forms of the advection term in equations (5) and (6), it is seen that the variation in ρ^* across the U -grid at the “e” and “w” faces of the “P” cell is correctly accounted for only in the conservative formulation. The non-conservative form simply attributes ρ_p^* to both faces which, in context to the west-east interface movement shown in Figure 1, incorrectly assigns ρ_e to the east face. Thus, the non-conservative formulation smears the ρ^* -field about the interface attributing a large value of ρ^* to the gas phase thereby enabling it to unrealistically decelerate the liquid.

IMPACT OF DENSITY TREATMENT ON THE PHYSICS OF WAVE-BREAKING

The first research question pertaining to how and why the physics of wave-breaking gets influenced by density treatment is addressed in the present section. Three scenarios have been considered of which two pertain to depth-induced breaking and one pertains to steepness-induced breaking.

Solitary wave breaking over a plane-sloping beach

The first problem involves a solitary wave ($H/d = 0.45$) propagating in $d = 1$ m deep water and breaking over a plane-sloping beach defined by the equation: $z = 15^{-1}(x - 5.225)$; the scenario has been adopted from the experiments of Li and Raichlen (2003). For the RANS simulations, a $25 \times 1 \times 2.5$ m³ domain is considered. Two uniform mesh designs have been selected: a coarse mesh ($1250 \times 1 \times 125$) for qualitative assessment of the breaking topology (cf. Figure 3) and a fine mesh ($2500 \times 1 \times 250$) for validation (cf. Figure 2).

The validation study is first carried out in which the topology of the plunging wave is compared against the experimental data of Li and Raichlen (2003); the same is reported at the top in Figure 2. It is seen that both non-conservative and conservative solvers yield nearly the same topology of the asymmetric shoaling crest in the initial stages. However, as the forward face of the plunging crest becomes nearly vertical, the non-conservative formulation begins to deviate from the experiment owing to excessive flattening of the top of the wave. This is followed by the formation of an unrealistically thick plunging jet having a much smaller curvature compared to the one observed experimentally. The conservative solver, on the other hand, is found to be highly accurate in terms of replicating the evolution of the plunging jet. Some minor flattening of the lower surface of the plunging jet observed in case of the conservative solver may be attributed to numerical surface tension effects emerging from the non-local nature of interface normal calculation in OS-CICSAM (Saincher and Sriram, 2022a).

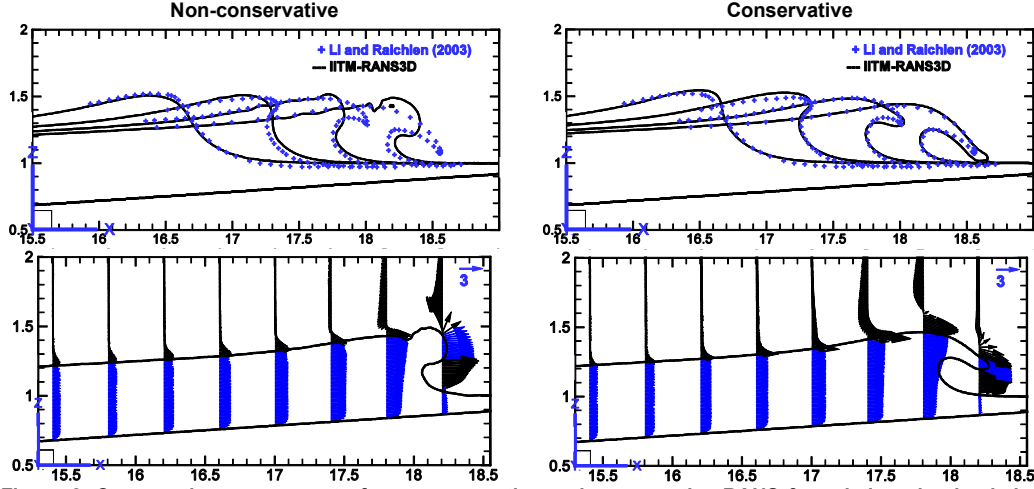


Figure 2. Comparative assessment of non-conservative and conservative RANS formulations in simulating solitary wave ($H/d = 0.45$) breaking over a plane-sloping beach: (top) evolution of breaking topology and (bottom) velocity vectors superimposed over the air-water interface with blue and black vectors lying in the water and air phases respectively.

The velocity vector field obtained in the air and water phases using both formulations is reported in Figure 2 (bottom) and also in Figure 3. In case of the non-conservative formulation, the vectors indicate that the velocity magnitude within the water phase decreases as one move towards the interface. This is not physical since it indicates that quiescent air, which is $800 \times$ lighter than water, is somehow able to decelerate the plunging crest. Said unphysical deceleration occurs due to the smearing of the ρ^* -field such that a very large density is attributed to cell-faces lying in air, immediately downstream to the plunging crest (cf. Figure 1).

In order to gain further insight into the question as to why the physics of breaking changes with density treatment, we take a cue from the work of Bussmann et al. (2002) and compare the non-conservative and conservative formulations in terms of a mass-inconsistency Δm which arises when the change in cell-mass is different from the net mass leaving the cell. The global mass-inconsistency, evaluated at a particular instant in time, for the entire domain is evaluated as:

$$\Delta m = \sum_{i=1}^{NX} \sum_{j=1}^{NY} \sum_{k=1}^{NZ} \left[\frac{(\rho_p^{t+\delta} - \rho_p^t) \delta x \delta y \delta z}{\text{increase of mass in "P"}} - \frac{\begin{aligned} &(\rho_w^t U_{i,j,k} - \rho_e^t U_{i+1,j,k}) \Delta t \delta y \delta z \\ &+ (\rho_s^t V_{i,j,k} - \rho_n^t V_{i,j+1,k}) \Delta t \delta x \delta z \\ &+ (\rho_b^t W_{i,j,k} - \rho_t^t W_{i,j,k+1}) \Delta t \delta x \delta y \end{aligned}}{\text{net mass entering "P"}} \right] \quad (8)$$

where, NX, NY, NZ are the total number of cells along the x, y, z directions respectively, $\delta x, \delta y, \delta z$ are the cell-sizes along the x, y, z directions respectively, δt is the time-step size, the subscripts e, w, n, s, t, b denote the "east", "west", "north", "south", "top" and "bottom" cell-faces respectively and the superscripts $t + \delta t, t$ denote the current and previous time levels respectively. In context to equation (8), the first term within the triple summation denotes the net increase in mass of a cell "P" over a time-step (computed by OS-CICSAM) whilst the remaining three terms denote the net mass entering the cell "P" (computed by momentum advection).

If the net increase doesn't balance the net entry, it indicates an inconsistency between mass and momentum transport (Bussmann et al., 2002). It is worth noting from equation (8) that there are two principal ways in which the mass-inconsistency may be manifested:

1. incorrect estimation of the face-densities in the interfacial region, and
2. the divergence of velocity not being "exactly zero" within the bulk of air and water phases.

In context to the above, it should be noted that the second contributing factor ($\vec{\nabla} \cdot \vec{V}$) is an inherent limitation stemming from numerical approximation of various terms in the Navier-Stokes equations and is thus present in both non-conservative and conservative formulations. This contribution can be reduced but cannot be eliminated entirely.

The time-variation of Δm over the entire course of the soliton-breaking simulation is reported at the center in Figure 3 and the same is correlated against the resulting topology of the overturning wave over the plane-sloping beach.

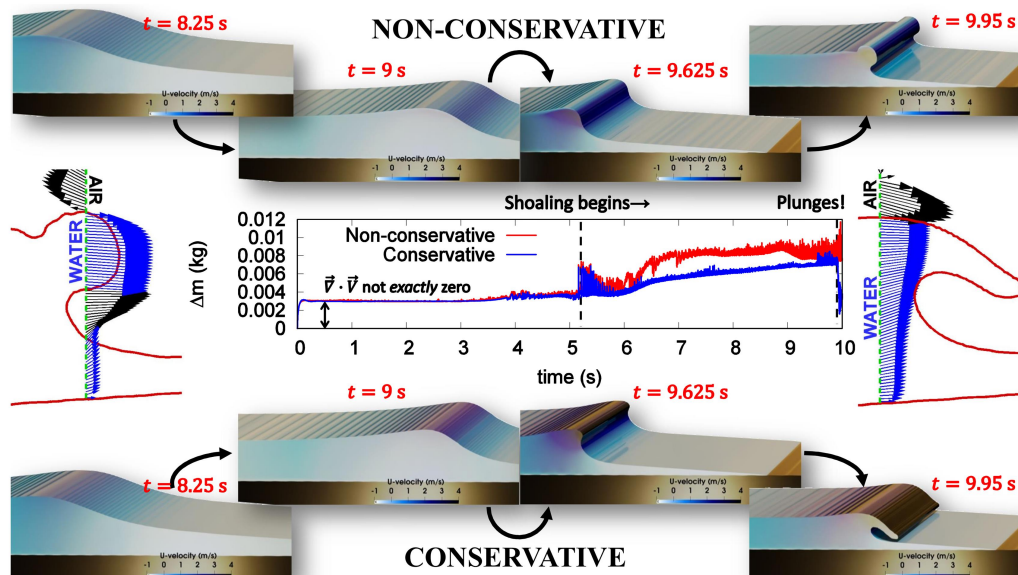


Figure 3. Evaluation of the mass-defect (Δm) over time for a solitary wave breaking over a plane sloping beach and correlating the same with the resulting topology of the plunging jet. The iso-volumes of water volume-fraction illustrating the overturning-wave have been colored by streamwise (U) velocity.

It is evident from Figure 3 that Δm is comparable for both advection formulations for $t \leq 5$ s. For $t > 5$ s, the wave begins to shoal over the beach and as the crest gradually becomes asymmetric, a strong west to east transport of the interface is established. If ρ^* were considered cell-centered, such west to east interface propagation over the staggered grid would result in ρ_ℓ being assigned to U -cell faces immediately downwind of the interface (cf. Figure 1). This gets reflected in a steeper increase in Δm for the non-conservative solver for $t \gtrsim 6$ s with its value being consistently greater than its conservative counterpart for the remainder of the simulation. Since Δm is solely generated in the interfacial region and the effect is accumulative, the end result is an unphysical attribution of mass to air just downwind of the shoaling wave. This decelerates the free-surface, causes the plunging jet to unnaturally thicken/flatten and delays the plunging altogether in case of the non-conservative solver.

Referring to Figure 3, it is interesting to note that the plunging event is marked by a sharp reduction in Δm ; the reduction is only seen for the conservative formulation because the plunging occurs after $t = 10$ s in case of the non-conservative solver. Although the exact numerical phenomenon causing the sharp reduction is not known at this juncture, we believe that the same is not caused by density treatment since the reduction was observed for both formulations. The sharp reduction has more to do with back-staggering of the momentum grid with respect to the pressure grid. During initial shoaling over the beach, the advection of the interface is predominantly 1-D (“west to east”) which results in a large build-up of fluxing errors. As the wave plunges, the interface transport becomes 2-D (“northwest to southeast”) and the accumulated shoreward fluxing errors gets compensated along the depthward direction.

Solitary wave breaking over a sloping ridge

The second problem involves a steep solitary wave ($H/d = 0.6$) propagating in $d = 1$ m deep water and breaking over a sloping ridge defined by: $z = 15^{-1}(x - 5.225)\text{sech}^2\{0.5(y - 2)\}$. The ridge is formed by modulating the plane-sloping beach from the first problem along the longshore direction using a sech^2 function. The scenario has been adopted from Grilli et al. (2001) wherein the problem was simulated using the (potential-flow-based) Boundary Element Method (BEM). For the RANS simulations, a $25 \times 4 \times 2.5$ m³ domain has been considered. Two uniform mesh designs have been selected: a coarse mesh ($1250 \times 50 \times 125$) for qualitative assessment of the breaking topology (cf. Figure 5) and a fine mesh ($2500 \times 101 \times 250$) for validation (cf. Figure 4).

The validation study is reported in Figure 4 wherein the topology of the shoaling wave obtained using IITM-RANS3D has been compared against the BEM simulations of Grilli et al. (2001). Since the bathymetry varies in both shoreward and longshore directions, the comparison is shown over the center as well as side(s) of the ridge. As evidenced from Figure 4, the conservative formulation achieves a closer agreement to the BEM simulations, especially at the center of the ridge where the curvature of

the overturning crest is greater; the non-conservative formulation yields a flattened crest. Nonetheless, since only the incipient overturning has been compared, the extent of disagreement between non-conservative RANS and BEM is lesser in contrast to that observed for the soliton breaking over the plane-sloping beach (cf. Figure 2). It is also believed that the reduction of the slope from 1:15 at the center to 1:36 at the sides results in a more gradual transition in the topology of the shoaling wave such that both formulations are rendered comparable during incipient breaking.

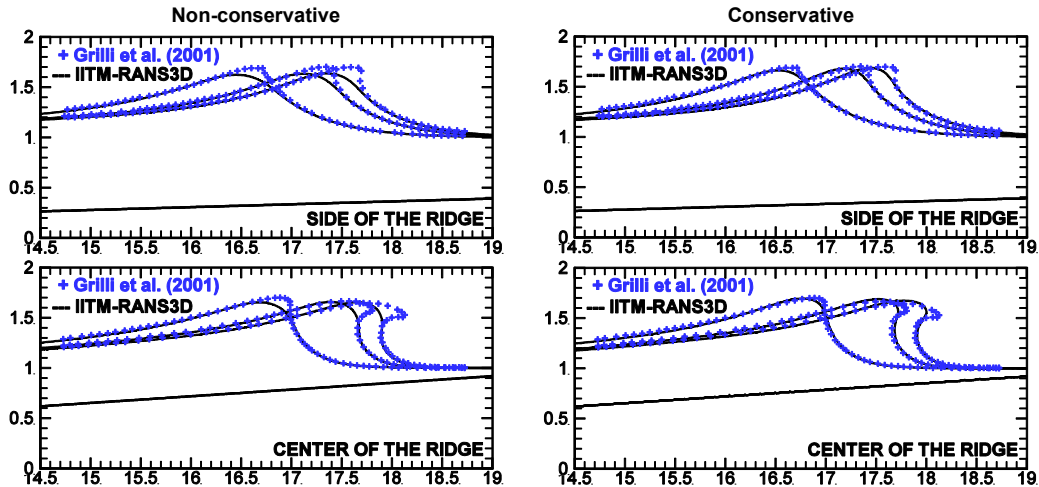


Figure 4. Comparative assessment of non-conservative and conservative RANS formulations in simulating steep solitary wave ($H/d = 0.6$) breaking over a sloping ridge illustrated through the evolution of breaking topology over: (top) side ($y = 0$ m ; 1:36 slope) and (bottom) center of the ridge ($y = 2$ m ; 1:15 slope).

The time-variation of Δm over the entire course of the soliton-breaking simulation is reported at the center in Figure 5 and the same is correlated against the resulting topology of the overturning wave over the sloping ridge. The velocity-vector fields near the over-turning crest are also shown in Figure 5 for both non-conservative and conservative formulations. The deceleration of the top surface of the overturning-crest in case of the non-conservative solver is clearly evidenced from the contours of U -velocity as well as the vector-field. In the case of complex bathymetry, not only does the crest deceleration result in a flattened jet, but also makes the central portion of the overturning wave to sag.

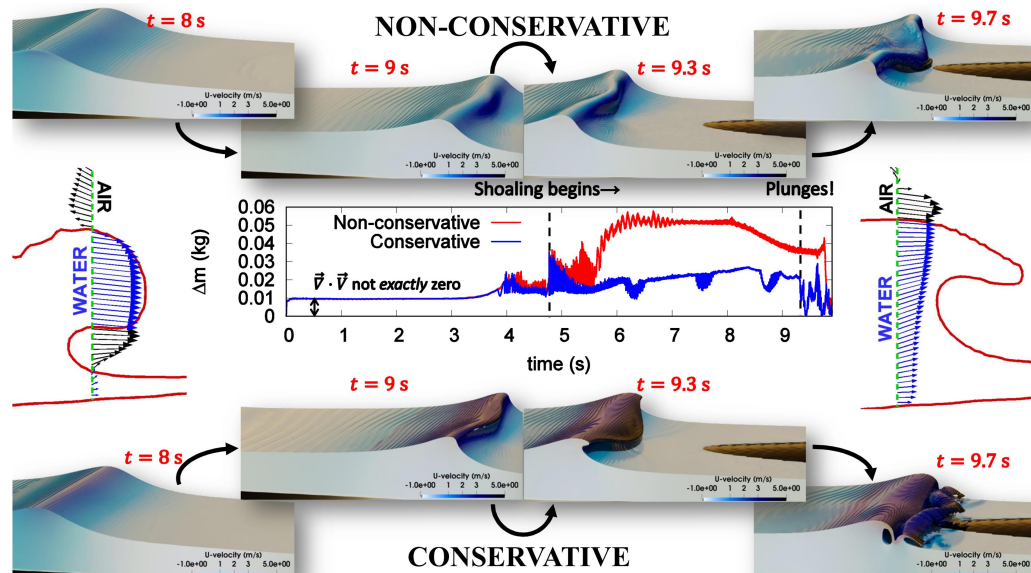


Figure 5. Evaluation of the mass-defect (Δm) over time for a solitary wave breaking over complex bathymetry (sloping ridge) and correlating the same with the resulting topology of the plunging jet. The iso-volumes of water volume-fraction illustrating the overturning-wave have been colored by streamwise (U) velocity.

Similar to the observations previously made from Figure 3, Δm is comparable for both advection formulations for $t \leq 5$ s. At $t \sim 5.5$ s, as the wave begins to shoal over the ridge, a steep rise is observed in the value of Δm for the non-conservative solver; the same remains $2 \times$ to $3 \times$ larger than its conservative counterpart for the remainder of the simulation. In fact, the accumulative effect of the mass-inconsistency is so strong in case of the non-conservative solver that it altogether prevents the wave from overturning at the sides of the ridge (cf. $t = 9.7$ s in Figure 5).

Unlike the first problem ($H/d = 0.45$ soliton), the steep reduction in the value of Δm during the later stages of the simulation, indicative of plunging, is seen to occur in both formulations. This is simply because the incident wave is comparatively steeper ($H/d = 0.6$) in this case and thus, despite the plunging being delayed by ~ 0.4 s in the non-conservative simulation (cf. Figure 5) the crest overturning completes before $t = 10$ s for both formulations.

Steepness induced breaking of a focusing wave

The third problem involves the generation of a train of wave packets in intermediate water using a piston-type wavemaker (WM) that focus at a point downstream of the wavemaker to form a steep wave that undergoes steepness-induced breaking.

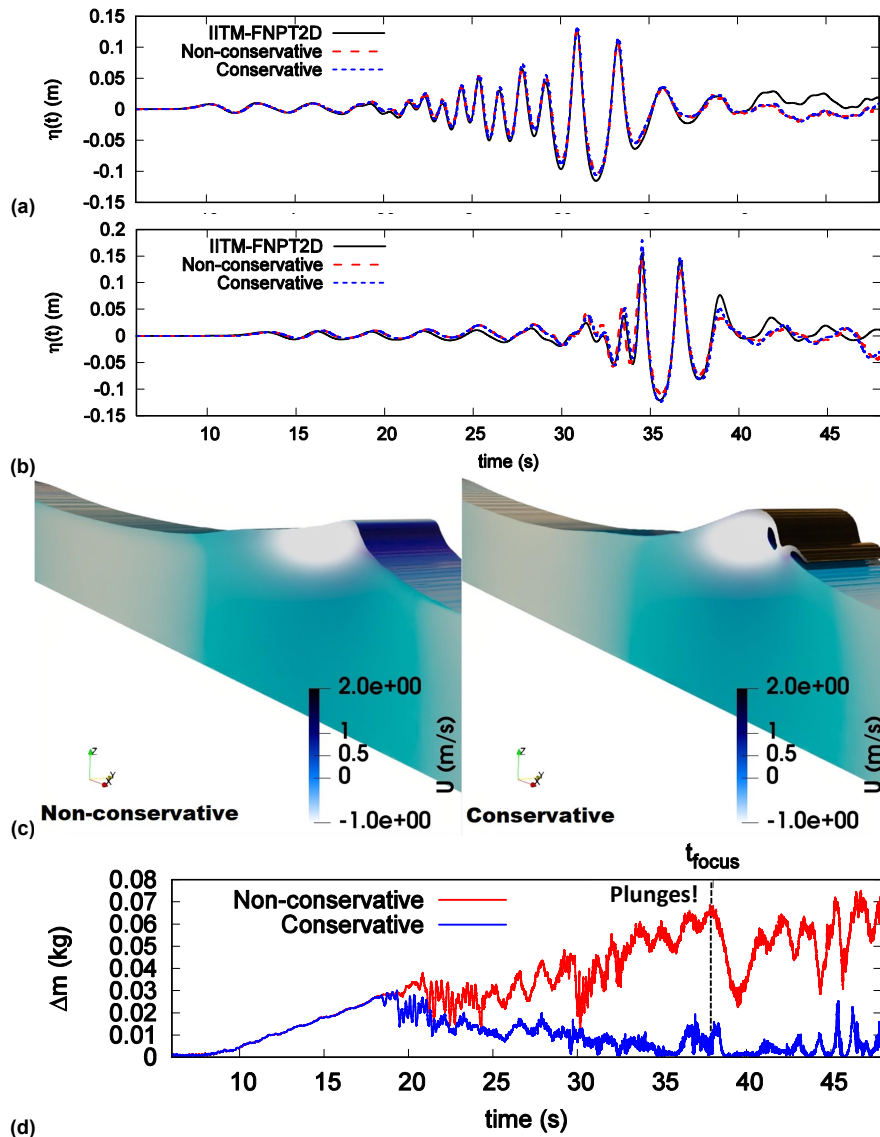


Figure 6. Comparative assessment of non-conservative and conservative RANS formulations for steepness-induced breaking of a focusing wave: validation of the free-surface elevation against FNPT simulations at (a) $x = WM + 12$ m, (b) $x = WM + 20$ m, (c) breaking topology colored by U -velocity and (d) mass-inconsistency.

The focused wave is generated through linear superposition of 32 wave packets in $d = 0.7$ m deep water. The wave packets have a constant steepness $ak = 0.01194$ where a is the amplitude and k is the circular wavenumber. The packets are equispaced within the frequency range $0.34 \text{ Hz} \leq f \leq 1.02 \text{ Hz}$ and are designed to focus $x \sim 25$ m downstream of the wavemaker at $t \sim 38$ s. The wave-paddle motion is prescribed using the second-order wavemaker theory proposed by Sriram et al. (2015).

The waves have been generated by directly inputting the wave-paddle motion to the potential-flow solver IITM-FNPT2D. The waves have been absorbed after $x = 20$ m (before they focus and break) so as to prevent numerical instability and the FNPT solution itself is extracted at $x = 10$ m and input to IITM-RANS3D. For the simulations, a $25 \times 1 \times 2 \text{ m}^3$ domain discretized using a $2500 \times 1 \times 125$ mesh (non-uniform in the depthward direction) has been considered. The RANS simulations have been executed upto a physical time of $t = 54$ s.

The results from the IITM-RANS3D simulations are reported in Figure 6. For the sake of validation, both non-conservative as well as conservative runs have been compared against the FNPT results at two wave-probe locations: $x = 12$ m and $x = 20$ m from the wavemaker. The comparisons are reported in Figures 6(a) and (b). In case of the first probe (cf. Figure 6(a)), nearly the same elevation time-series is obtained using both formulations and the RANS simulations show good agreement with FNPT. For the second probe (cf. Figure 6 (b)) which is closer to the focusing point, the elevation of the highest wave is slightly under-predicted by the non-conservative formulation. Thus, the momentum loss incurred by non-conservative RANS also results in numerical damping of steep waves.

The topology of the breaking wave in the near-field of the focusing point is shown in Figure 6(c). In case of the conservative formulation, the overturning of the wave-crest as well as the formation of the plunging jet and reactionary splash-up are accurately captured. In case of the non-conservative simulations, no overturning is observable and the crest elevation near the focusing location appears to have considerably diminished compared to the conservative solution. These observations lend considerable insight into the numerical behavior of RANS solvers for steepness-limited breaking in deep water. In case of the focusing wave, breaking is of a “milder nature” in that only the top portion of the crest overturns and breaks over a short distance. This is in stark contrast to depth-limited breaking of solitons (illustrated previously) wherein the whole crest overturns and breaks over a long distance. It appears that the former, milder form of breaking is more challenging to capture using a non-conservative solver. The tendency to flatten/reduce the curvature of the crest is so strong in this case that the overturning process is entirely not captured by non-conservative RANS.

The time-variation of the mass-inconsistency (Δm) has also been evaluated for the focused wave-breaking scenario; the same is reported in Figure 6(d). It is seen that Δm is equivalent across both formulations in the initial stages of the simulation. However, the two formulations deviate after $t \sim 18$ s with a steady build-up of Δm in case of the non-conservative formulation. This build-up further accelerates after $t \sim 30$ s to an extent that, at the instant of focusing ($t_{\text{focus}} = 38$ s), the mass-inconsistency is $\sim 7 \times$ greater in case of the non-conservative solver. Although there is a sharp reduction in Δm at t_{focus} , which is indicative of plunging, no crest overturning could be observed for non-conservative RANS. It seems likely that in this case, owing to the large Δm , the crest broke as a spilling or micro-scale breaking wave wherein there is minimal/no overturning but a 2-D (“northwest to southeast”) transport of momentum was nonetheless established which compensated the shoreward fluxing errors along the depthward direction.

INFLUENCE OF DENSITY TREATMENT ON WAVES IMPACTING A COASTAL STRUCTURE

The two RANS formulations have also been compared for a WSI problem involving a coastal structure. The scenario has been adopted from the large-scale (1:1) experiments carried out by Stagonas *et al.* (2020) wherein 0.7 m high waves having a period of 6 s propagating in 4.1 m deep water shoal over a 1:10 beach and interact with a recurved seawall. The results from both non-conservative and conservative IITM-RANS3D simulations are reported in Figure 7 in terms of the wave topology as well as the hydrodynamic pressure recorded on the vertical portion of the seawall.

It is evidenced from Figure 7 that the shape of the plunging jet formed close to the seawall is distorted in case of the non-conservative solver. More importantly, the interaction between the incident and reflected waves as well as the decelerating effect of air at the interface jointly leads to the formation of unphysical undulations on the free-surface (cf. Figure 7 (top)) which eventually destabilized the non-conservative simulation ($t \sim 71.5$ s). Thus, although the resulting hydrodynamic pressure trends may be comparable (cf. Figure 7 (bottom)), conservative RANS proved to be more stable for this violent wave-structure-interaction problem.

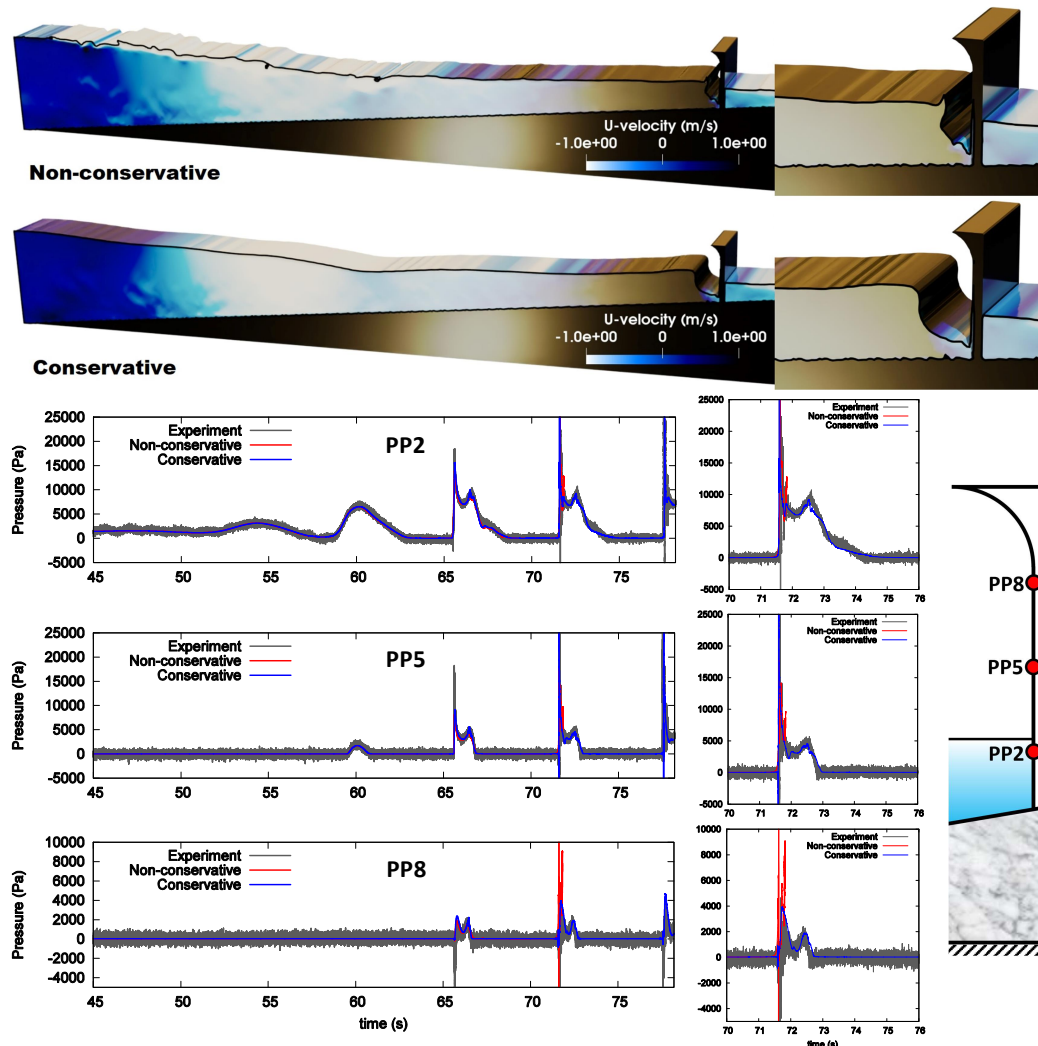


Figure 7. Comparative assessment of conservative and non-conservative RANS formulations for breaking waves impacting a seawall at prototype scale: (top) wave topology in the near-field of the structure colored by contours of streamwise (U) velocity and (bottom) time-variation of hydrodynamic pressure recorded at three representative probe locations.

CONCLUSIONS

In the present paper, a detailed comparative assessment of non-conservative and conservative RANS formulations for the simulation of depth-induced as well as steepness-induced wave-breaking and the simulation of breaking waves impacting a coastal structure is presented. The following major conclusions are drawn from the present work:

1. Multiphase RANS simulations of breaking waves are impacted by the strategy adopted for treating momentum advection.
2. The non-conservative formulation prescribes an unrealistically large density to the air-phase. This develops a strong inconsistency between the total increase in cell mass and the total mass entering the cell through its faces. The inconsistency is especially pronounced during shoaling.
3. The mass inconsistency causes a deceleration of the water phase at the interface leading to an unphysical, thick/flattened plunging jet.
4. The mass inconsistency can be considerably reduced through conservative treatment of advection thereby leading to physically realistic simulation of breaking; especially depth-limited breaking where overturning occurs over a large distance.
5. In case of the conservative formulation, mild flattening of the overturning jet/reduction in interfacial curvature may, in part, be attributable to numerical surface tension effects inherent to the volume-of-fluid method.

6. Both RANS formulations are found to be comparable for breaking waves impacting a seawall but the conservative formulation is found to be more stable from a numerical point of view.

ACKNOWLEDGMENTS

The first author acknowledges support from Institute Postdoctoral fellowship of IIT Madras. The authors acknowledge the use of the computing resources at HPCE, IIT Madras. The authors acknowledge technical discussions with Prof. Zhihua Xie (Cardiff University, UK) during implementation of the conservative solver.

REFERENCES

- Aggarwal, A., H. Bihs, D. Myrhaug, and M.A. Chella. 2019. Characteristics of breaking irregular wave forces on a monopile, *Applied Ocean Research*, ELSEVIER, 90, 101846.
- Aggarwal, A., M.A. Chella, H. Bihs, and D. Myrhaug. 2020. Properties of breaking irregular waves over slopes, *Ocean Engineering*, ELSEVIER, 216, 108098.
- Bussmann, M., D.B. Kothe and J.M. Sicilian. 2002. Modeling high density ratio incompressible interfacial flows, *ASME 2002 Joint U.S.-European Fluids Engineering Division Conference*, ASME, vol. 1, pp. 707-713.
- Chella, M.A., H. Bihs, D. Myrhaug, and M. Muskulus. 2017. Breaking solitary waves and breaking wave forces on a vertically mounted slender cylinder over an impermeable sloping seabed, *Journal of Ocean Engineering and Marine Energy*, SPRINGER, 3, 1-19.
- Chella, M.A., H. Bihs, and D. Myrhaug. 2019. Wave impact pressure and kinematics due to breaking wave impingement on a monopile, *Journal of Fluids and Structures*, ELSEVIER, 86, 94-123.
- Desmons, F., and M. Coquerelle. 2021. A generalized high-order momentum preserving (HOMP) method in the one-fluid model for incompressible two phase flows with high density ratio, *Journal of Computational Physics*, ELSEVIER, 437, 110322.
- Grilli, S.T., P. Guyenne, and F. Dias. 2001. A fully non-linear model for three-dimensional overturning waves over an arbitrary bottom, *International Journal for Numerical Methods in Fluids*, WILEY, 35, 829-867.
- Li, Y., and F. Raichlen. 2003. Energy Balance Model for Breaking Solitary Wave Runup, *Journal of Waterway, Port, Coastal, and Ocean Engineering*, ASCE, 129, 47-59.
- Mirzaei, I., and M. Passandideh-Fard. 2012. Modeling free surface flows in presence of an arbitrary moving object, *International Journal of Multiphase Flow*, ELSEVIER, 39, 216-226.
- Saincher, S., and J. Banerjee. 2018. Two-Phase Navier-Stokes Simulations of Plunging Breaking Waves, *Proceedings of the 7th International and 45th National Conference on Fluid Mechanics and Fluid Power (FMFP 2018 - held at IIT Bombay, India)*.
- Saincher, S., and V. Sriram. 2022a. An efficient operator-split CICSAM scheme for three-dimensional multiphase-flow problems on Cartesian grids, *Computers & Fluids*, ELSEVIER, 240, 105440.
- Saincher, S., and V. Sriram. 2022b. A three dimensional hybrid fully nonlinear potential flow and Navier Stokes model for wave structure interactions, *Ocean Engineering*, ELSEVIER, 266, 112770.
- Sriram, V., S.A. Sannasiraj, and V. Sundar. 2006. Simulation of 2-D nonlinear waves using finite element method with cubic spline approximation, *Journal of Fluids and Structures*, ELSEVIER, 22, 663-681.
- Sriram, V., Q.W. Ma, and T. Schlurmann. 2014. A hybrid method for modelling two dimensional non-breaking and breaking waves, *Journal of Computational Physics*, ELSEVIER, 272, 429-454.
- Sriram, V., T. Schlurmann, and S. Schimmels. 2015. Focused wave evolution using linear and second order wavemaker theory, *Applied Ocean Research*, ELSEVIER, 53, 279-296.
- Stagonas, D., R. Ravindar, V. Sriram, and S. Schimmels. 2020. Experimental evidence of the influence of recurves on wave loads at vertical seawalls, *Water*, MDPI, 12, 889.
- Xie, Z. 2011. Numerical study of breaking waves by a two-phase flow model, *International Journal for Numerical Methods in Fluids*, WILEY, 70, 246-268.
- Xie, Z. 2015. A two-phase flow model for three-dimensional breaking waves over complex topography, *Proceedings of the Royal Society A*, THE ROYAL SOCIETY, 471, 20150101.
- Xie, Z., and T. Stoesser. 2020. Two-phase flow simulation of breaking solitary waves over surface-piercing and submerged conical structures, *Ocean Engineering*, ELSEVIER, 213, 107679.
- Xie, Z., and P. Lin. 2022. Eulerian and Lagrangian transport by shallow-water breaking waves, *Physics of Fluids*, AIP, 34, 032116.